Bipolar Electrochemical Method for Dynamic *In Situ* Control of Single Metal Nanowire Growth

Marissa Wood and Bo Zhang*

Department of Chemistry, University of Washington, Seattle, Washington 98195, United States

ABSTRACT Fabrication plays a key role in determining the unique electrical, optical, and catalytic properties of metal nanowires. Here we present a bipolar electrochemical method for dynamically monitoring and controlling the rate of single metal nanowire growth *in situ* without a direct electrical connection. Solutions of a metal precursor and a reducing agent are placed on either side of a silica nanochannel, and a pair of electrodes is used to apply a tunable electric potential across the channel. Metal nanowire growth is initiated by chemical reduction when the two solutions meet and continues until the nanochannel is blocked by the formation of a short metal wire segment. Further growth is driven by a bipolar electrochemical mechanism which enables the reduction of metal precursor ions at one end of the nanowire and the oxidation of the reducing agent at the other. The growth rate is monitored in real time by simultaneously recording both the faradaic current and optical microscope video and can be adjusted accordingly by changing the applied electric potential. The resulting nanowire is solid, electrically insulated, and can be used as a bipolar nanoelectrode. This technique can be extended to other electrochemical systems, as well, and provides a confined reaction space for studying the dynamics of any process that can be optically or electrically monitored.

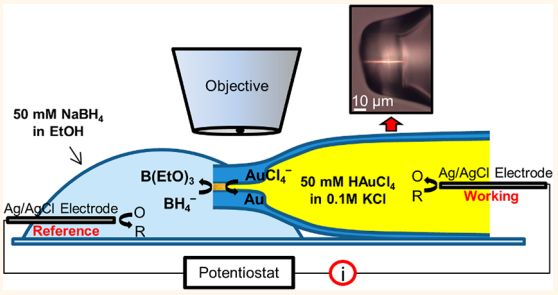

KEYWORDS: nanowire · metal deposition · nanoelectrode · bipolar electrochemistry · nanochannel · controlled fabrication · gold

Metal nanowires have garnered considerable research attention due to their unique electrical, optical, and catalytic properties, which make them well-suited for applications in nanoelectronics,[1−5] optics,[6−9] sensing,[10−13] and electrochemistry.[14−17] Since these properties are determined by the structure and crystallinity of the wire, controlled fabrication is critical for customization. While numerous synthesis techniques have been employed,[18−22] template-confined deposition[23−25] has emerged as one of the most popular due to two major advantages—it allows the morphology and location of metal growth to be precisely tailored by the template architecture, and it imposes transport limitations that help regulate growth kinetics.

Template-confined deposition can be carried out using either electrochemical or electroless techniques. In electrochemical deposition,[26−31] metal ions are reduced at a conductive surface on the template by an applied potential, which can be adjusted to tune growth rate and crystallinity. While this straightforward control enables high-quality unidirectional growth, it requires a direct electrical connection to the template, which is often difficult to establish on the nanoscale. Conversely, electroless deposition[32−35] occurs by direct chemical reduction and does not require an electrical connection or an applied potential, resulting in a considerably simpler setup that is more conducive to nanoscale fabrication. However, it often requires preactivation of the surface by several additional steps, and the growth rate and direction are less controllable. Ideally, the benefits of both techniques could be combined to yield a simple setup that requires no direct electrical connection or surface preactivation but maintains the control afforded by an externally applied potential.

Indeed, several recent reports have made exciting progress toward combining these advantages. For example, Drndic and coworkers[36] demonstrated the formation of a single gold nanoparticle inside a silicon nitride nanopore by chemical reduction,

* Address correspondence to zhang@chem.washington.edu.

Received for review July 30, 2014 and accepted February 19, 2015.

Published online February 19, 2015
10.1021/acsnano.5b00139

with the mixing of precursor solutions regulated by an applied electric field. However, this process is self-limiting, preventing further growth after the short pore length (*e.g.*, <30 nm) is blocked. Nanoparticles and nanowires have also been fabricated on a variety of conductive surfaces by using a supportive metal substrate with the appropriate redox potential to drive the reduction of metal ions in solution.[37−39] In addition, several studies have deposited metal between conductive microparticles or at the end of carbon micro/nanotubes by a wireless method known as bipolar electrodeposition, in which an applied electric field, rather than a direct electrical connection, is used to drive one-dimensional metal growth.[40−45] This approach requires a conductive starting substrate, which develops locally anodic and cathodic regions that facilitate coupled oxidation and reduction reactions. However, these substrates are difficult to fabricate and immobilize on the nanoscale, and the absence of a template eliminates the beneficial morphological and growth rate control that results from physical confinement. Furthermore, this method necessitates the application of very high potentials (up to kV), and the measured current cannot be used to directly monitor the reduction reaction since it is a combination of both faradaic and ionic current.

Wong and co-workers[46−48] and others[49] have reported the use of an innovative electroless process for the preparation of metal nanowire arrays that bypasses the necessity for an initial conductive starting substrate while maintaining the advantages of a template. This method uses direct chemical reduction to create metallic anchor segments in the pores of an array that can act as substrates for subsequent bipolar nanowire growth. This additional growth is believed to be driven by the difference between the redox potentials of the two precursor solutions, with electroneutrality maintained by both the flow of electrons through the nanowires themselves and the flow of electrolyte ions between the nanowires and the template walls.[47] However, this method does not produce electrically insulated wires, which are critical for many electrical and electrochemical applications. Moreover, the wires are frequently grown in arrays rather than individually. Although wires can be released from a templated array, manipulating single, free-standing wires for use in devices can be very challenging.

Most importantly, the deposition rate in a template-confined system is determined by how fast the redox species reach the surface of the growing wire, and in the above examples, this rate can only be controlled by changing the identities or concentrations of the redox species, which alters both the electrochemical driving force and the transport kinetics (due to changes in chemical potential). These parameters must be optimized for each experimental system and are set before the reaction begins. Consequently, they cannot be easily adjusted during the growth phase, even though deposition is a dynamic process, with local concentrations in constant flux as reagents are consumed and transport distances change with the shifting deposition site.

Here we present a bipolar electrochemical method for *in situ* control of single metal nanowire growth, showing that the deposition rate can be "wirelessly" and dynamically adjusted by applying an independently tunable electric field during the growth process. We demonstrate this enhanced control by depositing a single gold nanowire in a silica nanochannel template using a two-step chemical/bipolar electrochemical reduction mechanism while simultaneously monitoring both the current−time trace and optical microscope video of the growth process in real time. This method is highly reproducible, does not require a direct electrical connection, and can be carried out using an applied potential of less than 1 V. Scanning electron microscope (SEM) images show that the resulting wire is solid throughout its length. The use of a silica nanochannel template results in a single nanowire rather than a nanowire array, which allows us to accurately correlate electrical and optical observations with wire growth and regulate deposition without complications from ensemble effects. It also enables the insulated wire to be used as a bipolar nanoelectrode or to be easily manipulated and positioned for use in other applications that require isolated wires. Additionally, compared to the planar diffusion that occurs in an array configuration, radial diffusion to a single channel opening offers a fundamental transport advantage, aiding growth kinetics by increasing mass transport and avoiding quick depletion of the metal ions at the nanowire surface.

RESULTS AND DISCUSSION

Overview of Deposition Process. A diagram of our setup is shown in Figure 1a. A cylindrical-shaped silica nanochannel was fabricated at the end of a glass micropipette according to our previously published method[50] and employed as a template for metal deposition. Most nanochannels used in this work were between 200 and 400 nm in diameter and 20−50 μm in length, which enabled easy observation and imaging. However, we are able to make nanochannels with much smaller diameters, which could be employed to produce smaller diameter nanowires. The nanochannel was filled with 50 mM gold(III) chloride ($HAuCl_4$) in 0.1 M potassium chloride (KCl) and placed inside an empty solution chamber. A Ag/AgCl electrode was inserted into the supporting pipet of the nanochannel, and another was inserted into the solution chamber. The whole ensemble was positioned under an upright microscope in order to visually observe wire growth while simultaneously monitoring the resulting current between the electrodes. An initial potential of −0.6 V was applied to

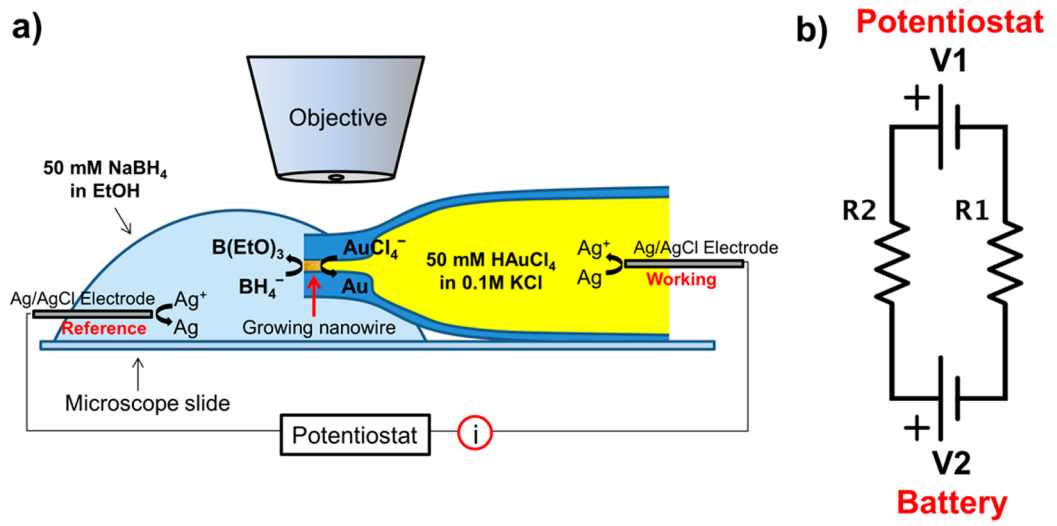

Figure 1. (a) Schematic of controlled nanowire deposition inside a silica nanochannel. When the two precursor solutions meet at the channel entrance, BH_4^- reduces $AuCl_4^-$ on contact, blocking the channel diameter. The redox potential difference between the two solutions creates an inherent battery potential that drives subsequent growth by a bipolar electrochemical mechanism, with $AuCl_4^-$ reduction at one end of the wire coupled to BH_4^- oxidation at the other. Electroneutrality is maintained by electron flow through the external circuit. The deposition rate can be dynamically controlled *in situ* by applying an independently tunable electric potential across the channel (*via* a potentiostat) to either enhance or oppose the battery potential. (b) Equivalent circuit diagram of our setup, where V1 is the external voltage, V2 is the spontaneous battery voltage, R1 is the resistance of the $HAuCl_4$ solution, and R2 is the resistance of the $NaBH_4$ solution.

the working electrode (defined as the electrode in the $AuCl_4^-$ solution), and a solution of 50 mM sodium borohydride ($NaBH_4$) in ethanol was introduced into the solution chamber to initiate the reaction. Ethanol was chosen instead of water because $NaBH_4$ reacts with different solvents to varying degrees, and the decomposition of $NaBH_4$ in ethanol is much slower than it is in water.

Gold growth proceeds in two stages: initial chemical reduction that generates gold particles until the channel is blocked, followed by bipolar electrochemical deposition that furthers the growth of the nanowire. Externally connecting the $AuCl_4^-$ and BH_4^- redox solutions creates a closed circuit, forming a simple battery that not only helps direct solution mixing during the initial chemical reduction phase but also drives the subsequent elongation of the wire. It is difficult to calculate the expected battery potential based on the standard redox potentials of the two solutions since the redox potential of BH_4^- is known to be solvent-dependent and is not reported in ethanol. However, we measured the cell potential to be ~1.2 V using a salt bridge to connect the two bulk redox solutions.

This spontaneous electrochemical potential is set by the identities and concentrations of the redox species, which cannot be easily adjusted during the growth process. However, these concentrations naturally fluctuate during the reaction as reagents are consumed and transport limitations change, causing simultaneous variations in both the battery potential and mass transport to the deposition site. Therefore, we introduce an independent, externally applied electric potential across the two Ag/AgCl electrodes that allows us to dynamically tune the total driving force of the system *in situ*. The equivalent circuit model for our setup is shown in Figure 1b. Depending on its polarity, this additional potential will either enhance or oppose the battery potential, providing a significant degree of control. This is particularly beneficial during the bipolar electrochemical deposition phase, in which growth of the short section of gold formed by chemical reduction is driven by coupled electrochemical oxidation and reduction reactions at opposite ends of the growing nanowire. Adjusting this externally applied potential therefore gives precise control over the growth rate of the gold during this period.

Chemical Reduction Phase. Initial gold deposition occurs by chemical reduction when the two redox solutions meet according to the following reaction:

$$8AuCl_4^- + 3BH_4^- + 9EtOH \rightarrow 8Au_{(s)} + 3B(EtO)_3 + 21H^+ + 32Cl^-$$

Ideally, this chemical reduction phase would be both fast and localized, immediately forming a short section of gold to plug the channel. While it is difficult to completely control the preliminary solution mixing, the electric potential across the channel provides a significant degree of regulation due to the identical charges of the two redox species. The $AuCl_4^-$ ions are electrophoretically driven into the channel, away from the working electrode in the pipet, while the BH_4^- ions migrate away from the channel toward the electrode in the external solution (defined as the reference electrode). Consequently, the initial interface of the two solutions is always located at the outside channel

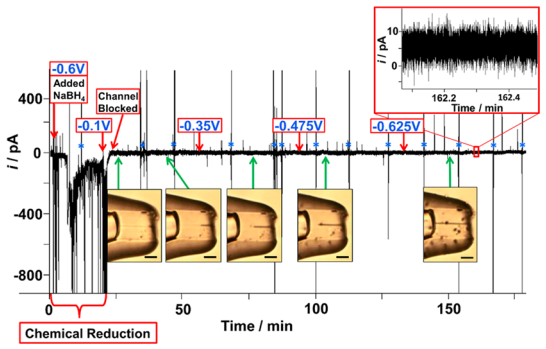

Figure 2. Current–time trace for gold deposition in a 293 nm diameter channel, along with accompanying optical microscope images at different time points during the growth process. The voltage values represent the external potential applied at the indicated times. An increase in ionic current is observed after adding $NaBH_4$ due to completion of the circuit through the channel. An external potential is applied during this initial stage to help direct solution mixing. Particle formation, dislodgment, and translocation through the channel are likely responsible for the transient current fluctuations observed until the channel is fully blocked (indicated by a current decay to zero). The subsequent small, positive faradaic current represents the onset of bipolar electrochemical deposition. As deposition proceeds, decreased mass transport resistance causes a natural increase in the deposition rate, which is countered by gradually increasing the magnitude of the externally applied potential to maintain an average rate of 3.1 nm/s. The blue asterisks indicate each time more $NaBH_4$ solution was added to the solution chamber. The large vertical current spikes correspond directly to these additions and are due to physical disruptions to the setup during these periods. The much smaller current spikes are due to footsteps and other small vibrations. Dark particles seen on the outside of the channel are small pieces of silicone rubber that have broken off from the chamber seal and do not affect the deposition process. All scale bars are 10 μm.

opening near the BH_4^- solution, which allows for consistent, reproducible control of both the starting point and direction of wire growth. It is important to note that the initial concentrations, while not easily controlled during the growth process, do play a vital role in determining how this chemical reduction phase proceeds. If the concentration of $NaBH_4$ is too high, there are too many nucleation sites, and deposition proceeds rapidly down the length of the channel without blocking the diameter. Similarly, if the concentration of $NaBH_4$ is too low, the rate of gold deposition is too slow to quickly block the channel, and growth likewise continues along the walls rather than across the width. Both situations produce porous wires. An additional transport hindrance is imposed on the $AuCl_4^-$ ions since they must travel through the channel to reach the deposition front. A 50 mM concentration of both $HAuCl_4$ and $NaBH_4$ was found to give a good balance between a reasonable number of nucleation sites and a fast enough chemical reduction rate.

Figure 2 shows a typical current–time trace with corresponding optical microscope images of the growing nanowire at different time points during the deposition. A time-lapse video of this growth is included in the Supporting Information. After $NaBH_4$ is initially added, a sudden increase in ionic current is observed as the solutions meet and the circuit is completed. The sign of the current is negative in accordance with the polarity of the applied potential. The current then immediately begins to decrease as gold is deposited at the channel entrance, shrinking the effective diameter of the channel. However, after this initial decrease, the current fluctuates significantly, reflecting the dynamic nature of this chemical reduction phase. Since BH_4^- reduces $AuCl_4^-$ on contact as soon as the solutions meet, there are multiple nucleation points for gold growth. Therefore, as Wong and co-workers have noted, this initial portion of the wire likely consists of many small gold particles connected together and is probably somewhat porous in nature.[47] This is confirmed by the SEM image of the outer section of the wire (Figure 4a), which shows aggregates of gold particles joined together. It is possible that initially formed gold nanoparticles or aggregates are easily dislodged from the channel before they can establish a strong anchor, causing the observed current fluctuations as they repeatedly form and detach from the channel entrance. Some of the particles may travel through and exit the channel, resulting in current fluctuations that resemble stochastic particle detection events observed in resistive-pulse sensing experiments.[51]

Eventually, these particles form a large and stable enough conglomerate to completely obstruct ion flow through the channel, as indicated by the subsequent current decrease to zero. Due to the nature of this initial chemical deposition, we have oriented our solutions with $AuCl_4^-$ on the inside and BH_4^- on the outside so that this more porous part of the wire is located near the outside of the channel and can be easily removed by focused ion beam (FIB) milling, polishing, or etching.

Solution Mixing Behavior without Potentiostat Control. While we have found that controlling the potential during this initial phase provides the best control over the rate of blockage formation, it is interesting to note that just the presence of a closed circuit (without the potentiostat) has an interesting regulatory effect on solution mixing. This is illustrated by comparing the behavior observed in two control experiments: one without an external electrical connection and one with only a wire connecting the two Ag/AgCl electrodes (no potentiostat). With no external connection between the redox solutions (Figure S2), their mixing is controlled solely by diffusion, and gold growth occurs exclusively by chemical reduction. As BH_4^- infiltrates the channel, rapid gold deposition takes place at multiple nucleation sites simultaneously, producing a porous wire that begins its growth at various locations in the channel. Consequently, the deposited gold does not initially block the channel diameter, instead continuing quickly down the sidewalls. As the wire approaches the end of the channel, the deposition rate

slows since the majority of the channel breadth has finally been blocked and mass transport through the channel is severely hindered. Conversely, the initial mixing behavior in the channel with the two Ag/AgCl electrodes connected only with a wire (Figure S3) shows a much slower and more controlled growth rate that is quite similar to the channel under potentiostat control shown in Figure 2.

Bipolar Electrochemical Deposition Phase. After the channel is fully obstructed and the solutions are no longer in physical contact, the growth mechanism switches from chemical reduction to bipolar electrochemical deposition. We have previously reported the unique behavior of closed bipolar systems, in which oxidation at one end of an insulated (closed) bipolar electrode is directly coupled to reduction at the other, allowing the reaction rate to be monitored by observing the faradaic current.[52,53] Therefore, once the deposited gold blocks the entire channel diameter, it acts as a bipolar electrode in the presence of a closed circuit, with $AuCl_4^-$ reduced at the cathodic end of the wire and BH_4^- oxidized at the anodic end. Since the spontaneous battery potential of ~1.2 V results in a growth rate that is often too fast to produce a high-quality wire, we apply the independent external potential in a direction contrary to the battery potential to decrease this driving force and reduce the deposition rate. The total potential across the gold wire is thus the difference between these two potentials. In order to maintain electroneutrality, oxidation of Ag must occur at the Ag/AgCl working electrode to balance the reduction of $AuCl_4^-$ at the cathodic end of the growing gold wire. Likewise, reduction of AgCl must occur at the Ag/AgCl reference electrode to balance the oxidation of BH_4^- at the anodic end. Therefore, the working electrode should record a positive faradaic current as deposition proceeds. The current trace in Figure 2 confirms that this is the case, showing a small positive current of ~6 pA as growth continues after the channel is initially blocked.

To further verify that gold deposition can occur by the described bipolar mechanism without physical contact between the metal precursor and the reducing agent, we performed a control experiment mimicking the setup in Figure 1, but with two changes: the $AuCl_4^-$ and BH_4^- solutions were placed in two separate beakers, and the two ends of the growing gold nanowire were represented by two glass-sealed Pt nanoelectrodes (one in each solution) connected to each other with a wire (Figure S4). Electrochemical measurements and SEM images confirm that when a potential was applied across the two Ag/AgCl electrodes, gold was deposited on the Pt nanoelectrode in the $AuCl_4^-$ solution even though it was not directly connected to the potentiostat, demonstrating that deposition occurred *via* a bipolar mechanism.

We can calculate the amount of gold deposited and the deposition rate for the channel shown in Figure 2 using Faraday's law, which states the relationship between the total charge passed (Q) and the number of moles of material deposited (N):[54]

$$Q = nFN \quad (1)$$

where n is the number of electrons transferred per redox molecule and F is Faraday's constant. The value of Q can be obtained by integrating the current−time curve in Figure 2 over just the bipolar electrodeposition phase and can be used to calculate the moles of deposited gold (N). When the dimensions of the channel are taken into account, this number can then be converted into an equivalent length and compared to the optical measurement of the channel length filled with gold during this time period. In order to make a more accurate optical comparison, we have chosen to analyze a slightly shorter time period within the bipolar electrodeposition phase, in which the starting and ending points of wire growth are clearly visible. Approximating the current as a constant value of 6 pA and integrating from 30 to 127 min gives 1.21×10^{-13} moles of deposited gold. This value can be converted into an equivalent volume using the density of gold and then an equivalent length by diving by the cross-sectional area of the channel. Thus, the length of gold deposited in the channel based on the faradaic current is calculated to be 18.2 μm, giving an average deposition rate of 3.1 nm/s. This length calculation agrees well with the value of 19.6 μm determined optically. The small discrepancy is likely due to the error associated with approximating the current as a constant value and error from the optical measurements, which are limited by the resolution of the microscope.

In addition to the average growth rate determined above, an instantaneous linear growth rate can be calculated from the faradaic current at any point during the deposition, providing insight into the growth conditions at that particular moment. For example, at 60 min, the current is 5.7 pA or 5.7×10^{-12} C/s, which can be used to calculate a volumetric rate and then divided by the cross-sectional area of the channel to give an instantaneous deposition rate of 3.0 nm/s. Therefore, recording the faradaic current allows the growth rate to be directly monitored and adjusted in real time.

As deposition proceeds and gold fills the channel, the mass transport resistance of the $AuCl_4^-$ ions decreases due to the diminishing distance between the bulk $AuCl_4^-$ solution and the recessed deposition site. Consequently, the enhanced migration of $AuCl_4^-$ ions results in an increased growth rate. This is observed in the control experiment performed using the same setup shown in Figure 1 but with no adjustment of the applied potential during the growth process (Figure S5), which shows a substantial increase in current as the growing wire nears the end of the channel, reaching a peak growth rate of 863 nm/s.

Therefore, in order to maintain a constant deposition rate, the externally applied potential must be continually increased in opposition to the battery potential to reduce the effective potential at the growing wire and slow the transport kinetics, as shown in Figure 2. It should be noted that this potential is controlled manually. While ideally a constant current would be maintained by galvanostatic control during this phase, our setup does not possess the capability to switch between potentiostatic (needed for the initial chemical reduction stage) and galvanostatic modes without first stopping the potentiostat to switch the settings, which could result in uneven growth and defects during this transition period.

We have further demonstrated this *in situ* control over the deposition rate by performing an experiment in which we intentionally changed the external potential by a significant amount in either direction several times during the growth process, causing large increases or decreases in the corresponding deposition rate and confirming that this externally applied potential can be used to dynamically tune the growth rate (Figure S6).

Wire growth is monitored under the microscope until it reaches the end of the channel. As we have shown in our previous papers on bipolar electrochemistry,[52,53] for electrochemical applications, it is advantageous to allow the inner surface of the gold wire to grow well beyond the end of the channel, as this increased size will help ensure that the current is limited by reactions occurring at the outer surface of the wire. This deposition method can also be used to fabricate other metal nanowires, as we have demonstrated for platinum (Figure S7).

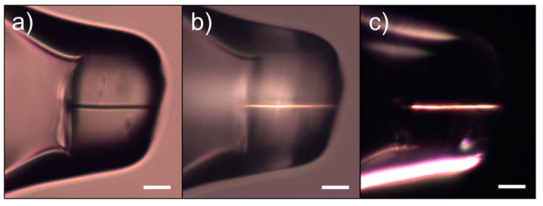

Figure 3. Optical microscope images of the completed wire from Figure 2: (a) bright-field, (b) reflectance, and (c) pseudo-dark-field. All scale bars are 10 μm.

Characterization by Microscopy and Cyclic Voltammetry. Optical microscope images of the finished wire are shown in Figure 3. The gold wire spans the entire length of the channel and appears solid throughout. An SEM image of the outside surface of a wire deposited under the same conditions is shown in Figure 4a. The unique gold structure reveals the initially disordered chemical reduction that occurs at the interface between the $AuCl_4^-$ and BH_4^- solutions. In order to further investigate the morphology and integrity of the wire, FIB milling was used to cut cross sections at three different points along the finished wire. These three locations and the corresponding SEM images of the cross sections are shown in Figure 4b–f. These images confirm that the wire is solid and maintains good contact with the glass throughout its length.

It is interesting to note that gold fills the entire channel diameter rather than propagating along the direction of the electric field from a single cross-sectional point, as has been observed in previous reports of open bipolar electrodeposition at conductive metal spheres and rings.[40,41] We believe that the primary difference lies in the profile of the deposition surface. In contrast to the curved deposition surfaces used in this prior work, we suspect that the profile of our growing nanowire surface is relatively flat due to the slow growth rate and the use of a closed bipolar electrode system. This promotes a relatively uniform distribution of electric potential at either end of the wire along the anodic and cathodic surfaces, respectively, allowing gold to fill the entire cross section.

While we were unable to obtain TEM images of the wire due to the thick surrounding glass, Karim and

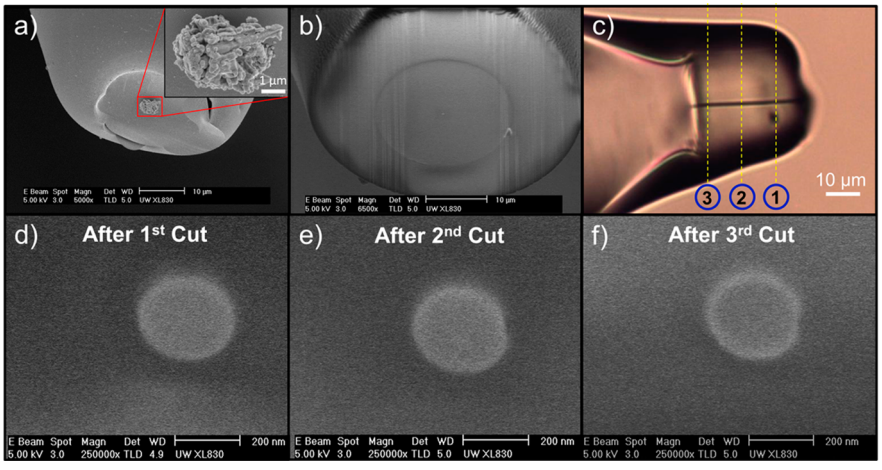

Figure 4. SEM images of a completed gold wire: (a) before cutting, showing the outer portion of the wire formed by chemical reduction; (b) after cutting. (d–f) Cross-section images after the first (d), second (e), and third (f) FIB cuts at the approximate locations indicated in (c), confirming that the wire is solid and maintains good contact with the glass throughout its length.

co-workers have noted that the type of cap that grows on top of the nanowire after it reaches the end of the confined nanochannel is indicative of wire crystallinity.[29] Figure S8 shows an SEM image of the cap grown on a nanowire *via* bipolar electrodeposition when the BH_4^- and $AuCl_4^-$ solution locations were reversed (in order to move the porous part of the wire formed by chemical reduction to the inside of the nanochannel and allow the section formed by controlled bipolar electrodeposition to grow through to the outside for easy imaging). Since the cap consists of an ordered collection of smaller wire-like protrusions rather than a single crystal, the nanowire is probably high-quality polycrystalline. However, this does not undermine its usefulness, and the crystallinity could likely be improved with further optimization.

Gold is a desirable electrode material because it is relatively inert but easy to functionalize for applications that require surface modification. However, it is difficult to fabricate single gold nanoelectrodes due to the challenge of establishing electrical contact and the low melting point of gold, which makes traditional laser-pulling methods used to fabricate platinum nanoelectrodes difficult.[55] Our method is therefore an excellent way to prepare gold nanoelectrodes. For a closed bipolar electrode, in which the nanowire is electrically insulated as it is here, all of the current in the system is carried through the nanowire. Therefore, the measured current can be directly and quantitatively correlated to redox reactions occurring at the nanowire itself. This is in contrast to an open bipolar system, in which the nanowire is surrounded by an electrolyte solution, and the measured current is a combination of the faradaic current carried through the nanowire and the ionic current carried through the solution.[56]

Cyclic voltammetry was performed to demonstrate the ability of the insulated gold wire to function as a bipolar nanoelectrode. The supporting pipet was filled with 10 mM ferricyanide in 0.1 M phosphate buffer at pH 7.4, while the outside was immersed in 2 mM ferrocenemethanol (FcMeOH) in 0.1 M phosphate buffer at pH 7.4. As we have discussed in our previous reports, provided that the current is sufficiently limited by one pole of the electrode (through either ample area or concentration differences between the two poles), there are no functional limitations to the closed bipolar setup, and a bipolar electrode can be used in the same way as a traditional electrode.[52,53] Since the inner face of the wire described here has a larger surface area and is in contact with a higher concentration redox solution, the current is limited by the oxidation of FcMeOH at the outer surface. A cyclic voltammogram (CV) is shown in Figure 5, along with the corresponding SEM image of the electrode after FIB cutting. The electrochemical response is nearly identical in shape and current magnitude to that expected from a traditional electrode. The radius of the electrode

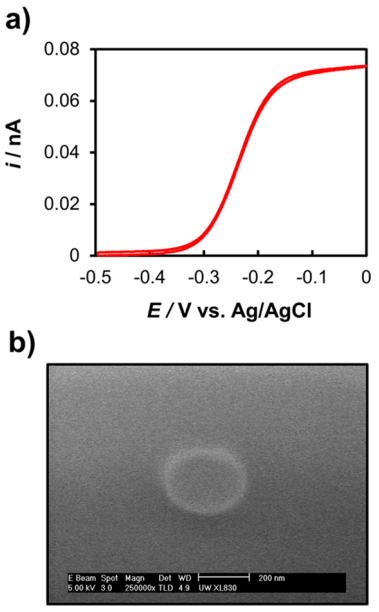

Figure 5. Demonstration of a deposited gold wire functioning as a bipolar nanoelectrode. (a) Cyclic voltammogram of the nanowire electrode in 2 mM FcMeOH in 0.1 M phosphate buffer, pH 7.4, at a scan rate of 10 mV/s. The inside of the supporting capillary was filled with 10 mM ferricyanide in 0.1 M phosphate buffer, pH 7.4. (b) Corresponding SEM image of the cross section confirming the 274 nm diameter calculated from the steady-state limiting current in (a).

can be calculated using the equation for the steady-state current (i_{ss}) at a disk ultra-microelectrode:[54]

$$i_{ss} = 4nFDC^*r \quad (2)$$

where n and F are previously defined, D is the diffusion coefficient (6.7×10^{-6} cm^2/s for FcMeOH),[52] C^* is the bulk concentration of the redox species, and r is the electrode radius. A steady-state limiting current of 73.5 pA corresponds to an electrode diameter of 274 nm, which matches well with the 279 nm diameter measured from the SEM image.

An important difference between the electrochemical response of a bipolar electrode and a traditional electrode is the position of the half-wave potential, $E_{1/2}$ (the potential when the current is half of its steady-state value), which is shifted in a bipolar setup. However, this shift is predictable, meaning that a bipolar electrode can still be used for catalytic studies and other experiments in which results are determined by monitoring the $E_{1/2}$ position. We have previously shown that the $E_{1/2}$ for a closed bipolar electrode shifts depending on the ratio between the anodic and cathodic steady-state limiting currents according to the following equation:[53]

$$E_{1/2} = (E_a^{o\prime} - E_c^{o\prime}) - \frac{RT}{nF}\ln\left(-2\left(\frac{i_{ss}^c}{i_{ss}^a}\right) - 1\right) \quad (3)$$

where $E_a^{o\prime}$ and $E_c^{o\prime}$ are the formal potentials for the reactions occurring at the anodic and cathodic poles,

R is the universal gas constant, T is the temperature, n and F are previously defined, and i^a_{ss} and i^c_{ss} are the maximum possible steady-state limiting currents at the anodic and cathodic poles, respectively. The cathodic current is defined as negative. The values of i^a_{ss} (73.5 pA) and $E_{1/2}$ (−0.24 V) can both be obtained from the CV. Solving for i^c_{ss} in eq 3 gives a maximum cathodic limiting current of −7.0 nA. Since the gold grows outward after reaching the end of the channel, the inner end of the wire can be approximated as a hemisphere rather than a disk, with the steady-state current given by[54]

$$i_{ss} = 2\pi nFDC^* r \quad (4)$$

The limiting current above corresponds to an inner hemisphere diameter of 3 μm, which is reasonable given that it is visible under the microscope. Therefore, we can calculate the diameters of both the outer and inner ends of the wire from a single CV. We have found that running repeated CVs often results in a loss of contact between the wire and the surface of the glass. We do not fully understand the nature of this disconnection, but we are currently working on surface modification procedures to improve adhesion.

CONCLUSIONS

We have presented a simple, highly reproducible method for dynamically controlling the rate of metal nanowire deposition *in situ*. This approach employs a combined chemical/bipolar electrochemical mechanism that does not require a direct electrical connection and is driven by the redox potential difference between solutions of a metal precursor and a reducing agent. When these solutions mix in a confined nanochannel template, a short metal nanowire is formed, creating a closed bipolar electrochemical cell that separates the reduction of metal precursor ions at one end of the nanowire from the oxidation of the reducing agent at the other. This bipolar process is monitored in real time by the faradaic current readout and optical microscopy and can be regulated by applying an independently tunable electric field across the nanowire, enabling precise "wireless" control over the deposition rate. We demonstrated this method by depositing a single gold nanowire in a silica nanochannel template and characterized the resulting wire by SEM and cyclic voltammetry, confirming that it is solid throughout its length and can be used as a bipolar nanoelectrode. The ability to directly monitor and control the deposition rate provides fundamental insight into the dynamics of metal growth under confinement. This procedure could be extended to other electrochemical systems as well and can be further tailored by modifying the template geometry, as the degree of confinement affects transport.[57]

Electrodes fabricated using this method could be easily modified to act as electrochemical sensors for the detection of specific analytes[58,59] or used to study single nanoparticle electrocatalysis if the electrode dimensions could be made sufficiently small.[17,60,61] With additional optimization, this process could also be used to fabricate small diameter tips for scanning electrochemical microscopy (SECM)[62] or nanowire arrays containing a known number of wires (so that the deposition rate could still be accurately monitored and controlled) for quick screening of potential catalysts[63] or use as high surface area sensors.[10−13] Since it provides a significant degree of control over the location, morphology, and growth rate of the wire without the need for a conductive starting substrate, this technique is particularly beneficial for applications that require precise positioning, such as fabrication of nanowires on a patterned chip for microfluidic electrochemical sensors[64,65] or deposition of metal catalysts used in the synthesis of other inorganic nanowires.[66] With further development, it could potentially also be extended to more complex processes, such as the deposition of binary semiconductors for photovoltaic and other optoelectronic applications.[67] Although transport and conductivity limitations would present additional challenges, the ability to tune the applied potential would allow significant control over the elemental composition and electronic properties of the resulting semiconductor. In addition, the miniature reaction chamber created by the channel is ideal for studying the confined dynamics of any process that can be optically or electrically monitored.

METHODS

Chemicals and Materials. All aqueous solutions were prepared using >18 MΩ·cm water from a Barnstead Nanopure water purification system. Ethanol (Decon Laboratories, Inc., 200 proof), potassium chloride (KCl, Macron Chemicals), sodium chloride (NaCl, JT Baker), potassium ferricyanide ($K_3Fe(CN)_6$, Sigma-Aldrich), ferrocenemethanol (FcMeOH, Sigma-Aldrich), monopotassium phosphate (KH_2PO_4, JT Baker), dipotassium phosphate (K_2HPO_4, JT Baker), chloroplatinic acid (H_2PtCl_6, Sigma-Aldrich), and sodium borohydride ($NaBH_4$, Sigma-Aldrich) were all reagent grade and were used without further purification. Gold(III) chloride ($HAuCl_4$) was purchased from Salt Lake Metals (1% solution by weight, 99.99% purity). Silica capillary tubing (o.d. = 1.0 mm, i.d. = 0.3 mm) was obtained from Sutter Instrument Company, and silica microcapillaries (o.d. = 0.35 mm, i.d. = 20 μm) were from Polymicro Inc.

Nanochannel Fabrication. Nanochannels were prepared according to a previously reported process.[50] Briefly, a small piece of silica microcapillary (o.d. = 0.35 mm, i.d. = 20 μm) was first sealed inside a larger silica capillary (o.d. = 1.0 mm, i.d. = 0.3 mm) using a laser-based micropipette puller (P-2000, Sutter Instrument Company). The diameter of the inner capillary was decreased through a series of heating and cooling cycles under vacuum before the whole ensemble was pulled into two long nanotips. A nanotip was inserted into a larger diameter borosilicate holder pipet under an optical microscope until the end

could be seen protruding ~5–10 μm from the holder opening. It was then passed very quickly through a natural gas flame to seal a small section to the walls of the holder. The remainder of the tip was broken off and removed, leaving only the small sealed segment containing the nanochannel. The protruding end was cut off under the microscope using a razor blade.

Gold Deposition. After resistance measurements in 0.1 M KCl were performed to determine the nanochannel diameter,[50] the supporting pipet was filled with 50 mM $HAuCl_4$ in 0.1 M KCl and inserted into a home-built polycarbonate solution chamber attached to a glass microscope slide. A thin glass coverslip was set on top of the chamber, and two Ag/AgCl electrodes were placed inside of the supporting pipet (designated as the working electrode) and the solution chamber (designated as the reference electrode). Pictures of the solution chamber as well as a more detailed description are included in the Supporting Information (Figure S1). The whole ensemble was then positioned under a 20× microscope objective (Nikon) inside a Faraday cage. A potential of −0.6 V was applied across the open circuit, after which ~1 mL of 50 mM $NaBH_4$ in ethanol was slowly added to the solution chamber to initiate the reaction. Although the solution chamber is covered, there is a small area open to the air where the $NaBH_4$ is added. As time proceeds, two things occur: first, ethanol evaporates, and the solution must be replenished; second, bubbles generated by the slow decomposition of $NaBH_4$ in ethanol aggregate to form large bubbles that can cover the channel opening. A dark shadow can be seen in the optical microscope image when the solvent front begins to approach the channel (either from evaporation or a large bubble), indicating the need for more $NaBH_4$ solution to either replenish the solution or dislodge the bubble. The applied potential was adjusted manually to accelerate blockage formation during the initial chemical reduction phase and to maintain a near constant current value during subsequent bipolar deposition.

Current–time traces were acquired using an Axopatch 200B high-impedance amplifier (Molecular Devices, Inc.) and a Digidata 1440A digitizer (Molecular Devices, Inc.) interfaced to a Dell computer. A 1.0 kHz low-pass filter was applied to the amplifier during data acquisition, but no further filtering was performed. An optical video was simultaneously recorded with the OCView7 software package using a Nikon Eclipse E600 microscope connected to a CCD camera (OptixCam Summit Series).

Resistance Measurements and Cyclic Voltammetry. Current–voltage responses were measured using a Chem-Clamp potentiostat (Dagan, Inc.) and a PAR 175 universal function generator (Princeton Applied Research). The potentiostat was interfaced to a Dell computer through a PCI-6251 data acquisition board (National Instruments) *via* a BNC-2090 analog breakout box (National Instruments). The data were recorded using a custom program written in LabView 8.5 (National Instruments). All measurements were conducted inside a Faraday cage in a one-compartment, two-electrode cell with a Ag/AgCl working electrode inside the supporting pipet and a Ag/AgCl reference electrode in the outside solution.

Focused Ion Beam and Scanning Electron Microscopy. Focused ion beam milling and SEM imaging were performed using a FEI XL830 dual beam FIB/SEM instrument.

Conflict of Interest: The authors declare no competing financial interest.

Supporting Information Available: A more detailed description of the experimental setup as well as current–time traces, optical microscope images, and SEM images for control experiments and platinum wire deposition, and a time-lapse video of nanowire growth. This material is available free of charge *via* the Internet at http://pubs.acs.org.

Acknowledgment. The authors gratefully acknowledge financial support from the Defense Threat Reduction Agency (DTRA) (Contract No. HDTRA1-11-1-0005) and the AFOSR MURI (FA9550-14-1-0003). The authors also thank R. Hao and B. Wood for their insightful discussions, and S. Percival for providing the Pt nanoelectrodes used in the control experiment. FIB milling and SEM imaging were performed by R. Hao at the University of Washington NanoTech User Facility, a member of the NSF National Nanotechnology Infrastructure Network (NNIN).

REFERENCES AND NOTES

1. Lu, W.; Lieber, C. M. Nanoelectronics from the Bottom Up. *Nat. Mater.* **2007**, *6*, 841–850.
2. Kwiat, M.; Cohen, S.; Pevzner, A.; Patolsky, F. Large-Scale Ordered 1D-Nanomaterials Arrays: Assembly or Not? *Nano Today* **2013**, *8*, 677–694.
3. Kovtyukhova, N. I.; Mallouk, T. E. Nanowires as Building Blocks for Self-Assembling Logic and Memory Circuits. *Chem.—Eur. J.* **2002**, *8*, 4355–4363.
4. Schvartzman, M.; Tsivion, D.; Mahalu, D.; Raslin, O.; Joselevich, E. Self-Integration of Nanowires into Circuits *via* Guided Growth. *Proc. Natl. Acad. Sci. U.S.A.* **2013**, *110*, 15195–15200.
5. Morrow, T. J.; Li, M. W.; Kim, J.; Mayer, T. S.; Keating, C. D. Programmed Assembly of DNA-Coated Nanowire Devices. *Science* **2009**, *323*, 352–352.
6. Lal, S.; Hafner, J. H.; Halas, N. J.; Link, S.; Nordlander, P. Noble Metal Nanowires: From Plasmon Waveguides to Passive and Active Devices. *Acc. Chem. Res.* **2012**, *45*, 1887–1895.
7. Guo, X.; Ying, Y.; Tong, L. Photonic Nanowires: from Subwavelength Waveguides to Optical Sensors. *Acc. Chem. Res.* **2014**, *47*, 656–666.
8. Wei, H.; Xu, H. Nanowire-Based Plasmonic Waveguides and Devices for Integrated Nanophotonic Circuits. *Nanophotonics* **2012**, *1*, 155–169.
9. Hou, X.; Zhang, X.; Chen, S.; Fang, Y.; Li, N.; Zhai, X.; Liu, Y. Size-Controlled Synthesis of Au Nanoparticles and Nanowires and Their Application as SERS Substrates. *Colloids Surf., A* **2011**, *384*, 345–351.
10. Ongaro, M.; Ugo, P. Bioelectroanalysis with Nanoelectrode Ensembles and Arrays. *Anal. Bioanal. Chem.* **2013**, *405*, 3715–3729.
11. Viswanathan, S.; Rani, C.; Delerue-Matos, C. Ultrasensitive Detection of Ovarian Cancer Marker Using Immunoliposomes and Gold Nanoelectrodes. *Anal. Chim. Acta* **2012**, *726*, 79–84.
12. Mardegan, A.; Scopece, P.; Lamberti, F.; Meneghetti, M.; Moretto, L. M.; Ugo, P. Electroanalysis of Trace Inorganic Arsenic with Gold Nanoelectrode Ensembles. *Electroanalysis* **2012**, *24*, 798–806.
13. Silvestrini, M.; Fruk, L.; Ugo, P. Functionalized Ensembles of Nanoelectrodes as Affinity Biosensors for DNA Hybridization Detection. *Biosens. Bioelectron.* **2013**, *40*, 265–270.
14. Oja, S. M.; Wood, M.; Zhang, B. Nanoscale Electrochemistry. *Anal. Chem.* **2013**, *85*, 473–486.
15. Murray, R. W. Nanoelectrochemistry: Metal Nanoparticles, Nanoelectrodes, and Nanopores. *Chem. Rev.* **2008**, *108*, 2688–2720.
16. Yeh, J. I.; Shi, H. B. Nanoelectrodes for Biological Measurements. *Wiley Interdiscip. Rev. Nanomed. Nanobiotechnol.* **2010**, *2*, 176–188.
17. Li, Y.; Cox, J. T.; Zhang, B. Electrochemical Responses and Electrocatalysis at Single Au Nanoparticles. *J. Am. Chem. Soc.* **2010**, *132*, 3047–3054.
18. Li, N.; Zhao, P.; Astruc, D. Anisotropic Gold Nanoparticles: Synthesis, Properties, Applications, and Toxicity. *Angew. Chem., Int. Ed.* **2014**, *53*, 1756–1789.
19. Vigderman, L.; Khanal, B. P.; Zubarev, E. R. Functional Gold Nanorods: Synthesis, Self-Assembly, and Sensing Applications. *Adv. Mater.* **2012**, *24*, 4811–4841.
20. Kim, F.; Sohn, K.; Wu, J.; Huang, J. Chemical Synthesis of Gold Nanowires in Acidic Solutions. *J. Am. Chem. Soc.* **2008**, *130*, 14442–14443.
21. Xu, Q.; Rioux, R. M.; Dickey, M. D.; Whitesides, G. M. Nanoskiving: A New Method To Produce Arrays of Nanostructures. *Acc. Chem. Res.* **2008**, *41*, 1566–1577.
22. Menke, E. J.; Thompson, M. A.; Xiang, C.; Yang, L. C.; Penner, R. M. Lithographically Patterned Nanowire Electrodeposition. *Nat. Mater.* **2006**, *5*, 914–919.
23. Hurst, S. J.; Payne, E. K.; Qin, L. D.; Mirkin, C. A. Multisegmented One-Dimensional Nanorods Prepared by Hard-Template Synthetic Methods. *Angew. Chem., Int. Ed.* **2006**, *45*, 2672–2692.

24. Wirtz, M.; Martin, C. R. Template-Fabricated Gold Nanowires and Nanotubes. *Adv. Mater.* **2003**, *15*, 455–458.
25. Piao, Y.; Kim, H. Fabrication of Nanostructured Materials Using Porous Alumina Template and Their Applications for Sensing and Electrocatalysis. *J. Nanosci. Nanotechnol.* **2009**, *9*, 2215–2233.
26. Penner, R. M.; Martin, C. R. Preparation and Electrochemical Characterization of Ultramicroelectrode Ensembles. *Anal. Chem.* **1987**, *59*, 2625–2630.
27. Tian, M. L.; Wang, J. U.; Kurtz, J.; Mallouk, T. E.; Chan, M. H. W. Electrochemical Growth of Single-Crystal Metal Nanowires *via* a Two-Dimensional Nucleation and Growth Mechanism. *Nano Lett.* **2003**, *3*, 919–923.
28. Toimil-Molares, M. E. Characterization and Properties of Micro- and Nanowires of Controlled Size, Composition, and Geometry Fabricated by Electrodeposition and Ion-Track Technology. *Beilstein J. Nanotechnol.* **2012**, *3*, 860–883.
29. Karim, S.; Toimil-Molares, M. E.; Maurer, F.; Miehe, G.; Ensinger, W.; Liu, J.; Cornelius, T. W.; Neumann, R. Synthesis of Gold Nanowires with Controlled Crystallographic Characteristics. *Appl. Phys. A: Mater. Sci. Process.* **2006**, *84*, 403–407.
30. Liu, J.; Duan, J. L.; Toimil-Molares, E.; Karim, S.; Cornelius, T. W.; Dobrev, D.; Yao, H. J.; Sun, Y. M.; Hou, M. D.; Mo, D.; Wang, Z. G.; Neumann, R. Electrochemical Fabrication of Single-Crystalline and Polycrystalline Au Nanowires: The Influence of Deposition Parameters. *Nanotechnology* **2006**, *17*, 1922–1926.
31. Wu, Z.; Zhang, Y.; Du, K. A Simple and Efficient Combined AC–DC Electrodeposition Method for Fabrication of Highly Ordered Au Nanowires in AAO Template. *Appl. Surf. Sci.* **2013**, *265*, 149–156.
32. Menon, V. P.; Martin, C. R. Fabrication and Evaluation of Nanoelectrode Ensembles. *Anal. Chem.* **1995**, *67*, 1920–1928.
33. De Leo, M.; Pereira, F. C.; Moretto, L. M.; Scopece, P.; Polizzi, S.; Ugo, P. Towards a Better Understanding of Gold Electroless Deposition in Track-Etched Templates. *Chem. Mater.* **2007**, *19*, 5955–5964.
34. Krishnamoorthy, K.; Zoski, C. G. Fabrication of 3D Gold Nanoelectrode Ensembles by Chemical Etching. *Anal. Chem.* **2005**, *77*, 5068–5071.
35. Kan, C. X.; Cai, W. P.; Li, Z. S.; Fu, G. H.; Zhang, L. D. Reduction Effect of Pore Wall and Formation of Au Nanowires Inside Monolithic Mesoporous Silica. *Chem. Phys. Lett.* **2003**, *382*, 318–324.
36. Venta, K.; Wanunu, M.; Drndic, M. Electrically Controlled Nanoparticle Synthesis Inside Nanopores. *Nano Lett.* **2013**, *13*, 423–429.
37. Qu, L. T.; Dai, L. M. Substrate-Enhanced Electroless Deposition of Metal Nanoparticles on Carbon Nanotubes. *J. Am. Chem. Soc.* **2005**, *127*, 10806–10807.
38. Inguanta, R.; Piazza, S.; Sunseri, C. Novel Procedure for the Template Synthesis of Metal Nanostructures. *Electrochem. Commun.* **2008**, *10*, 506–509.
39. Xu, Q.; Meng, G.; Wu, X.; Wei, Q.; Kong, M.; Zhu, X.; Chu, Z. A Generic Approach to Desired Metallic Nanowires inside Native Porous Alumina Template *via* Redox Reaction. *Chem. Mater.* **2009**, *21*, 2397–2402.
40. Bradley, J.-C.; Chen, H.-S.; Crawford, J.; Eckert, J.; Ernazarova, K.; Kurzeja, T.; Lin, M.; McGee, M.; Nadler, W.; Stephens, S. Creating Electrical Contacts Between Metal Particles Using Directed Electrochemical Growth. *Nature.* **1997**, *389*, 268–271.
41. Bradley, J.-C.; Crawford, J.; Ernazarova, K.; McGee, M.; Stephens, S. Wire Formation on Circuit Boards Using Spatially Coupled Bipolar Electrochemistry. *Adv. Mater.* **1997**, *9*, 1168–1171.
42. Bradley, J.-C.; Babu, S.; Carroll, B.; Mittal, A. A Study of Spatially Coupled Bipolar Electrochemistry on the Submicrometer Scale: Colloidal Particles on Surfaces and Cylinders in Nuclear-Track Etched Membranes. *J. Electroanal. Chem.* **2002**, *522*, 75–85.
43. Warakulwit, C.; Nguyen, T.; Majimel, J.; Delville, M.-H.; Lapeyre, V.; Garrigue, P.; Ravaine, V.; Limtrakul, J.; Kuhn, A. Dissymmetric Carbon Nanotubes by Bipolar Electrochemistry. *Nano Lett.* **2008**, *8*, 500–504.
44. Fattah, Z.; Garrigue, P.; Lapeyre, V.; Kuhn, A.; Bouffier, L. Controlled Orientation of Asymmetric Copper Deposits on Carbon Microobjects by Bipolar Electrochemistry. *J. Phys. Chem. C* **2012**, *116*, 22021–22027.
45. Loget, G.; Roche, J.; Kuhn, A. True Bulk Synthesis of Janus Objects by Bipolar Electrochemistry. *Adv. Mater.* **2012**, *24*, 5111–5116.
46. Zhou, H. J.; Zhou, W. P.; Adzic, R. R.; Wong, S. S. Enhanced Electrocatalytic Performance of One-Dimensional Metal Nanowires and Arrays Generated *via* an Ambient, Surfactantless Synthesis. *J. Phys. Chem. C* **2009**, *113*, 5460–5466.
47. Koenigsmann, C.; Santulli, A. C.; Sutter, E.; Wong, S. S. Ambient Surfactantless Synthesis, Growth Mechanism, and Size-Dependent Electrocatalytic Behavior of High-Quality, Single Crystalline Palladium Nanowires. *ACS Nano* **2011**, *5*, 7471–7487.
48. Koenigsmann, C.; Tan, Z.; Peng, H.; Sutter, E.; Jacobskind, J.; Wong, S. S. Multifunctional Nanochemistry: Ambient, Electroless, Template-Based Synthesis and Characterization of Segmented Bimetallic Pd/Au and Pd/Pt Nanowires as High-Performance Electrocatalysts and Nanomotors. *Isr. J. Chem.* **2012**, *52*, 1090–1103.
49. Sharabani, R.; Reuveni, S.; Noy, G.; Shapira, E.; Sadeh, S.; Selzer, Y. Fabrication of Very High Aspect Ratio Metal Nanowires by a Self-Propulsion Mechanism. *Nano Lett.* **2008**, *8*, 1169–1173.
50. Zhang, B.; Wood, M.; Lee, H. A Silica Nanochannel and Its Applications in Sensing and Molecular Transport. *Anal. Chem.* **2009**, *81*, 5541–5548.
51. Henriquez, R. R.; Ito, T.; Sun, L.; Crooks, R. M. The Resurgence of Coulter Counting for Analyzing Nanoscale Objects. *Analyst* **2004**, *129*, 478–482.
52. Guerrette, J. P.; Oja, S. M.; Zhang, B. Coupled Electrochemical Reactions at Bipolar Microelectrodes and Nanoelectrodes. *Anal. Chem.* **2012**, *84*, 1609–1616.
53. Cox, J. T.; Guerrette, J. P.; Zhang, B. Steady-State Voltammetry of a Microelectrode in a Closed Bipolar Cell. *Anal. Chem.* **2012**, *84*, 8797–8804.
54. Bard, A. J.; Faulkner, L. R. *Electrochemical Methods: Fundamentals and Applications*, 2nd ed.; John Wiley & Sons, Inc.: New York, 2001.
55. Cox, J. T.; Zhang, B. Nanoelectrodes: Recent Advances and New Directions. *Annu. Rev. Anal. Chem.* **2012**, *5*, 253–272.
56. Fosdick, S. E.; Knust, K. N.; Scida, K.; Crooks, R. M. Bipolar Electrochemistry. *Angew. Chem., Int. Ed.* **2013**, *52*, 10438–10456.
57. Sparreboom, W.; van den Berg, A.; Eijkel, J. C. T. Principles and Applications of Nanofluidic Transport. *Nat. Nanotechnol.* **2009**, *4*, 713–720.
58. Salamifar, S. E.; Lai, R. Y. Fabrication of Electrochemical DNA Sensors on Gold-Modified Recessed Platinum Nanoelectrodes. *Anal. Chem.* **2014**, *86*, 2849–2852.
59. Adams, K. L.; Jena, B. K.; Percival, S. J.; Zhang, B. Highly Sensitive Detection of Exocytotic Dopamine Release Using a Gold-Nanoparticle-Network Microelectrode. *Anal. Chem.* **2011**, *83*, 920–927.
60. Park, J. H.; Thorgaard, S. N.; Zhang, B.; Bard, A. J. Single Particle Detection by Area Amplification: Single Wall Carbon Nanotube Attachment to a Nanoelectrode. *J. Am. Chem. Soc.* **2013**, *135*, 5258–5261.
61. Fernández, J. L.; Walsh, D. A.; Bard, A. J. Thermodynamic Guidelines for the Design of Bimetallic Catalysts for Oxygen Electroreduction and Rapid Screening by Scanning Electrochemical Microscopy. *J. Am. Chem. Soc.* **2005**, *127*, 357–365.
62. Amemiya, S.; Bard, A. J.; Fan, F.-R. F.; Mirkin, M. V.; Unwin, P. R. Scanning Electrochemical Microscopy. *Annu. Rev. Anal. Chem.* **2008**, *1*, 95–131.
63. Fosdick, S. E.; Crooks, R. M. Bipolar Electrodes for Rapid Screening of Electrocatalysts. *J. Am. Chem. Soc.* **2012**, *134*, 863–866.
64. Dawson, K.; Wahl, A.; Barry, S.; Barrett, C.; Sassiat, N.; Quinn, A. J.; O'Riordan, A. Fully Integrated On-Chip Nano-Electrochemical

Devices for Electroanalytical Applications. *Electrochim. Acta* **2014**, *115*, 239–246.
65. Chen, A.; Tsao, M.-J.; Chuang, J.-F.; Lin, C.-H. Electrochemical Determination of Verapamil with a Microchip Embedded with Gold Nanoelectrode Ensemble Electrodes. *Electrochim. Acta* **2013**, *89*, 700–707.
66. Barth, S.; Hernandez-Ramirez, F.; Holmes, J. D.; Romano-Rodriguez, A. Synthesis and Applications of One-Dimensional Semiconductors. *Prog. Mater. Sci.* **2010**, *55*, 563–627.
67. Lincot, D. Electrodeposition of Semiconductors. *Thin Solid Films* **2005**, *487*, 40–48.